5672–5687 *Nucleic Acids Research, 2022, Vol. 50, No. 10* *Published online 30 May 2022*
https://doi.org/10.1093/nar/gkac447

RNF4 controls the extent of replication fork reversal to preserve genome stability

Linli Ding [1,†], Yi Luo[1,†], Tian Tian[2,†], Xu Chen[1,†], Yulan Yang[1,†], Min Bu[1], Jinhua Han[1], Bing Yang[1], Haiyan Yan[3], Ting Liu[4], Mengjie Wu[5], Guofei Zhang[6], Yipeng Xu[7], Shaoxing Zhu[7], Michael S.Y. Huen [8], Genxiang Mao[9] and Jun Huang [9,10,*]

[1]The MOE Key Laboratory of Biosystems Homeostasis & Protection and Innovation Center for Cell Signaling Network, Life Sciences Institute, Zhejiang University, Hangzhou 310058, Zhejiang, China, [2]The Eighth Affiliated Hospital, Sun Yat-Sen University, Shenzhen 518033, Guangdong, China, [3]School of Medicine, Zhejiang University City of College, Hangzhou 310015, Zhejiang, China, [4]Department of Cell Biology, and Department of General Surgery of Sir Run Run Shaw Hospital, Zhejiang University School of Medicine, Hangzhou 310058, Zhejiang, China, [5]The Affiliated Hospital of Stomatology, School of Stomatology, Zhejiang University School of Medicine and Key laboratory of Oral Biomedical Research of Zhejiang Province, Hangzhou 310058, Zhejiang, China, [6]Department of Thoracic Surgery, The Second Affiliated Hospital, Zhejiang University School of Medicine, Hangzhou 310058, Zhejiang, China, [7]Department of Urology, Cancer Hospital of the University of Chinese Academy of Sciences, Zhejiang Cancer Hospital, Hangzhou 310058, Zhejiang, China, [8]Department of Anatomy, The University of Hong Kong, Hong Kong, China, [9]Zhejiang Provincial Key Lab of Geriatrics and Geriatrics Institute of Zhejiang Province, Department of Geriatrics, Zhejiang Hospital, Hangzhou 310030, Zhejiang, China and [10]Zhejiang Provincial Key Laboratory of Cancer Molecular Cell Biology, Life Sciences Institute, Zhejiang University, Hangzhou 310058, Zhejiang, China

Received March 14, 2022; Revised May 09, 2022; Editorial Decision May 10, 2022; Accepted May 15, 2022

ABSTRACT

Replication fork reversal occurs via a two-step process that entails reversal initiation and reversal extension. DNA topoisomerase IIalpha (TOP2A) facilitates extensive fork reversal, on one hand through resolving the topological stress generated by the initial reversal, on the other hand via its role in recruiting the SUMO-targeted DNA translocase PICH to stalled forks in a manner that is dependent on its SUMOylation by the SUMO E3 ligase ZATT. However, how TOP2A activities at stalled forks are precisely regulated remains poorly understood. Here we show that, upon replication stress, the SUMO-targeted ubiquitin E3 ligase RNF4 accumulates at stalled forks and targets SUMOylated TOP2A for ubiquitination and degradation. Downregulation of RNF4 resulted in aberrant activation of the ZATT–TOP2A–PICH complex at stalled forks, which in turn led to excessive reversal and elevated frequencies of fork collapse. These results uncover a previously unidentified regulatory mechanism that regulates TOP2A activities at stalled forks and thus the extent of fork reversal.

INTRODUCTION

Faithful transmission of genetic material from parent to offsprings is critical for maintaining genome integrity, and relies on the accurate duplication of chromosomal DNA during the S-phase of cell cycle (1–5). However, the progression of replication forks is frequently challenged by diverse endogenous or exogenous stresses, such as unrepaired DNA lesions, difficult-to-replicate DNA sequences, DNA secondary structures, and replication-transcription collisions (1–5). To deal with these potentially deleterious events associated with DNA replication, cells have equipped with multiple mechanisms to metabolize stressed replication forks in order to preserve fork integrity (1–5).

A key protective mechanism against replication stress in higher eukaryotic cells is replication fork reversal, in which the two extruded nascent DNA strands anneal to form a Holliday junction (HJ)-like structure (6–8). It is now known that replication fork reversal is carried out via a two-step process (9). In the first step, the RAD51 recombinase cooperates with multiple fork remodelers, including SMARCAL1/HARP, HLTF and ZRANB3, to initiate limited fork reversal, thereby introducing positive supercoils into the newly synthesized sister chromatids to prevent further reversal of the stalled forks (6–16). In the second step, the resulting topological stress is removed by

*To whom correspondence should be addressed. Email: jhuang@zju.edu.cn
†The authors wish it to be known that, in their opinion, the first five authors should be regarded as Joint First Authors.

TOP2A (9). Meanwhile, TOP2A is SUMOylated by the SUMO E3 ligase ZATT (also known as ZNF451), which in turn facilitates the recruitment of the SUMO-targeted DNA translocase PICH to stalled forks to drive extensive fork reversal (9). Extensive fork reversal catalyzed by the ZATT–TOP2A–PICH protein complex prevents unscheduled fork restart, and is thus crucial for maintenance of genomic stability and cell survival under conditions of replication stress (9). In addition to the above-mentioned enzymes, DNA helicases FBH1, BLM, WRN, RECQ5, DNA translocases RAD54 and FANCM, and RAD51 paralogs have also been implicated in the fork reversal process, although their precise functions are not fully understood (17–23). While extensive fork reversal may be beneficial for the stabilization of stalled forks, uncontrolled and excessive fork reversal can lead to fork collapse and genomic instability. For instance, suppression of RAD52 or RADX, or over-activation of SMARCAL1 causes excessive fork reversal, which can result in uncontrolled degradation of nascent DNA and collapse of stalled replication forks (24–26). However, the mechanisms by which cells precisely control the extent of replication fork reversal at stalled replication forks remain poorly understood.

RING finger protein 4 (RNF4) belongs to a small group of RING finger E3 ubiquitin ligases that are collectively coined Small ubiquitin-related modifier (SUMO)-Targeted Ubiquitin Ligases (STUbLs) (27–29). RNF4 recognizes and binds to SUMOylated proteins via its N-terminal SUMO-interacting motifs (SIMs), and catalyzes their poly-ubiquitination via its C-terminal RING domain (27–29). In most cases, SUMO-dependent poly-ubiquitylation by RNF4 results in proteasome-mediated protein degradation (30–33). For example, RNF4 targets SUMO-modified MDC1 for poly-ubiquitination and subsequent degradation, thereby regulating the assembly/disassembly of DNA damage response (DDR) proteins at DNA damage sites (34–37). In addition to MDC1, several other DDR factors, such as FANCD2/FANCI, RPA, CtIP and BRCA1 have also been reported to be substrates of RNF4 (35,37–39). However, although several lines of evidence have revealed the importance of RNF4 in maintaining genomic integrity, whether and how RNF4 contributes to the stabilization of stalled replication forks are currently poorly understood. Here we report that RNF4 ubiquitinates SUMOylated TOP2A in response to replication stress, thereby regulating its proteasome-dependent turnover at stalled forks and extent of fork reversal. We found that RNF4-deficient cells exhibit aberrant activation of the ZATT–TOP2A–PICH protein complex at stalled forks, which in turn leads to uncontrolled excessive fork reversal and increased rates of stalled fork collapse. Our findings thus provide new insights into the molecular mechanism that regulates the extent of fork reversal and stalled fork stability.

MATERIALS AND METHODS

Antibodies and chemicals

Rabbit polyclonal anti-RNF4 (WB dilution: 1:1000), anti-PICH (WB dilution: 1:500; immunostaining dilution: 1:10 000) and anti-Ubc9 (WB dilution: 1:500) were produced by immunizing rabbits with GST-RNF4, GST-PICH (amino acids 791–1000), and GST-Ubc9 fusion proteins purified from *Escherichia coli* (Hangzhou HuaAn Biotechnology Co., Ltd.). Mouse monoclonal anti-53BP1 (immunostaining dilution: 1:500) was produced by immunizing mice with amino acids 149–259 of human 53BP1 (Abmart Shanghai Co., Ltd.). Anti-tubulin (M20005S, WB dilution: 1:5000), anti-GFP (M20004M, WB dilution: 1:1000) and anti-Myc (M20002S, WB dilution: 1:5000; immunostaining dilution: 1:20 000) antibodies were purchased from Abmart. Anti-TOP2A (ab52934, WB dilution: 1:10 000), anti-RPA2 (ab2175, immunostaining dilution: 1:2000), and anti-CIdU/BrdU (ab6326, immunostaining dilution: 1:500) antibodies were purchased from Abcam. Anti-TOP2A (M042-3, immunostaining dilution: 1:100 000) was purchased from MBL International. Anti-H3 (04-928, WB dilution: 1:5000) and anti-ubiquitin (05-944, clone: P4D1-A11, WB dilution: 1:1000) antibodies were purchased from EMD Millipore. Anti-HA (3724S, WB dilution: 1:1000) and anti-PCNA (PC10) (sc-56, WB dilution: 1:1000) antibodies were purchased from Cell Signaling Technology and Santa Cruz Biotechnology, respectively. Anti-Flag (M2, WB dilution: 1:5000, immunostaining dilution: 1:10 000) and anti-His (GNI4110-HS, WB dilution: 1:1000) antibodies were purchased from Sigma-Aldrich and GNI GROUP LTD, respectively. Anti-ZATT (A305-177A, WB dilution: 1:3000), anti-BRCA2 (A303-434A, WB dilution: 1:2000) and anti-Biotin (150-109A, immunostaining dilution: 1:3000) antibodies were purchased from Bethyl. Anti-IdU/BrdU (B44) (347580, immunostaining dilution: 1:500) antibody was purchased from BD Biosciences. Rhodamine conjugated goat anti-mouse IgG (15-001-003, immunostaining dilution: 1:500) and anti-biotin (200-002-211, immunostaining dilution: 1:4000) antibodies were purchased from Jackson ImmunoResearch. Alexan Fluor 488 Donkey anti-Rat IgG (A-21208, immunostaining dilution: 1:400) was purchased from Life technologies. Colcemid (C3915) and Etoposide were purchased from Sigma-Aldrich. Cyclohexamide (HY-12320) were purchased from MedChemExpress.

Cell culture and lentiviral transduction

HEK293T and HeLa cells were grown in Dulbecco's modified Eagle's medium (DMEM) supplemented with 10% fetal bovine serum (FBS) plus 1% penicillin–streptomycin antibiotics at 37°C in a humidified atmosphere containing 5% CO_2. All cells used in this study were grown under sterile conditions and routinely tested for mycoplasma contamination. Lentiviruses were produced by co-transfection of the His-ubiquitin or His-SUMO2 lentiviral plasmid with the packaging plasmids (pMD2G and pSPAX2) into HEK293T cells, and lentiviral supernatants were collected after 48 h. Infected cells were selected with 2 μg/ml puromycin after transduction.

Plasmids and transfection

GFP-tagged TOP2A and Flag-tagged ZATT were provided by Dr Fangwei Wang (Zhejiang University) and Dr Xinhua Feng (Zhejiang University), respectively. Point

mutations in the TOP2A or ZATT sequence were introduced by PCR-based site-directed mutagenesis. RNF4-WT, RNF4-ΔSIM and RNF4-CS constructs were previously described (39). cDNA encoding human RNF8 was cloned into pDONOR201 gateway entry vector (Invitrogen) and then recombined into a SFB-tagged (S tag, Flag epitope tag, and Streptavidin-binding peptide tag) destination vector. 10× His-tagged SUMO2, 10× His-tagged SUMO2-ΔGG, HA-tagged SUMO2, HA-tagged SUMO2-ΔGG, 10× His-tagged Ub, 10× His-tagged Ub-ΔGG were cloned into a lentivirus vector using MultiF Seamless Assembly Mix (ABclonal). All constructs were sequenced to confirm fidelity. Plasmid transfections were performed with polyethyleneimine.

Coimmunoprecipitation

To immunoprecipitate ectopically expressed SFB-tagged proteins, transfected HEK293T cells were harvested, lysed, and sonicated in NETN buffer (20 mM Tris–HCl [pH 8.0], 100 mM NaCl, 1 mM EDTA and 0.5% Nonidet P-40) containing protease inhibitors (1 μg/ml aprotinin and leupeptin). The lysates were centrifuged at 14 000g for 5 min, and the resulting supernatants were incubated with S-protein beads for 3 h at 4°C. After washing three times with NETN buffer, the resin-bound proteins were eluted by boiling in 2× SDS loading buffer and analyzed by SDS-PAGE. To immunoprecipitate the endogenous proteins, HeLa cells were collected, lysed, and sonicated in NETN buffer containing protease inhibitors. The lysates were centrifuged at 14 000 g for 5 min at 4°C, and the resulting supernatants were incubated with protein A–Sepharose coupled with 2 μg of the indicated antibodies for 3 h at 4°C. After washing three times with NETN buffer, the resin-bound proteins were eluted by boiling in 2× SDS loading buffer and analyzed by SDS-PAGE.

RNAi

All siRNAs used in this study were chemically synthesized by RuiBo. The siRNAs sequences are as follows: Ubc9 siRNA#1: 5′-UGCGCCAUUCCAGGAAAGAdTdT-3′; and Ubc9 siRNA#2: 5′-GUAAAUUCGAACCACCAUUdTdT-3′; ZATT siRNA#1, 5′-GCAGAAUUCAGGACACAAA dTdT-3′; ZATT siRNA#2, 5′-GAGUUAACAAGGAAAGAUAdTdT-3′; TOP2A siRNA#1, 5′-CCACGAAUAACCAUAGAAAdTdT-3′; TOP2A siRNA#2, 5′-UUCUGACAGACAACUUUCUU-3′; RNF4 siRNA#1: 5′-CUCAGGUACUGUCAGUUGUdTdT-3′; RNF4 siRNA#2: 5′-CCAUCUGCAUGGACGGAUAdTdT-3′; BRCA2 siRNA, 5′-GAAGAAUGCAGGUUUAAUA-3′ and control siRNA, 5′-UUCAAUAAAUUCUUGAGGUUU-3′. The siRNA-resistant wild-type and mutant RNF4 plasmids were constructed by substituting ten nucleotides in the RNF4 siRNA#2-targeting region (C378G, T379A, C380G, A381T, T384A, T387A, C390G, A391T, G392C and T396C). For siRNA transfection, cells were transfected twice at a 24-h interval with the indicated siRNAs using Lipofectamine RNAiMAX (Invitrogen) according to the manufacturer's protocol.

iPOND

iPOND was performed as previously described (40). Briefly, HEK293T cells were pulse-labeled with 10 μM EdU for 15 min. For pulse-chase experiments with thymidine, EdU-labeled cells were washed once with fresh medium to remove the EdU, then chased into 10 μM thymidine for 1 h. Cells were then left untreated or treated with 4 mM HU for 3 h, cross-linked with 1% formaldehyde for 20 min, quenched with 0.125 M glycine, and washed three times with PBS. Collected cell pellets were resuspended and permeabilized with 0.25% Triton X-100, washed once with ice-cold 0.5% BSA and once with PBS, and then incubated with a click reaction buffer (10 mM sodium ascorbate, 2 mM $CuSO_4$, and 10 μM biotin azide) for 80 min. After washing once with ice-cold 0.5% BSA and once with PBS, cells were resuspended and sonicated in lysis buffer (1% SDS, 50 mM Tris [pH 8.0]) containing protease inhibitors. The lysates were centrifuged, filtered, and diluted 1:1 with ice-cold PBS. Biotin conjugated DNA-protein complexes were captured using Streptavidin agarose resin (Millipore), and captured complexes were washed once with ice-cold lysis buffer, once with 1M NaCl, and twice with ice-cold lysis buffer. Proteins associated with nascent DNA were eluted by boiling in 2 × SDS Laemmli buffer (4% SDS, 20% glycerol, 125 mM Tris [pH 6.8], 0.1% (w/v) bromophenol blue and 0.25 M dithiothreitol) at 95°C for 20 min and analyzed by SDS-PAGE.

In situ proximity ligation assay

HeLa cells were pulse-labeled with 10 μM EdU for 15 min followed by treatment with 4 mM HU for 3 h. After washing with PBS, cells were permeabilized with 0.5% Triton X-100 for 10 min at 4°C, washed with PBS, fixed with 3% formaldehyde/2% sucrose in PBS at room temperature for 10 min, washed with PBS, and blocked with 3% BSA in PBS for 30 min. After blocking, cells were subjected to Click-iT reaction to conjugate biotin to EdU and then incubated with primary antibodies at 4°C overnight. Proximity ligation assays were performed by using Duolink In Situ Red Starter kit (Sigma-Aldrich) according to the manufacturer's protocol. Images were obtained using a Nikon Eclipse 80i Microscope equipped with a Plan Fluor 60× oil objective (NA 0.5–1.25; Nikon) and analyzed with NIS-Elements basic research imaging software (Nikon).

DNA fiber analysis

For measuring replication fork restart, HeLa cells were pulse-labeled with 50 μM IdU for 30 min, treated with 4 mM HU for 3 h, and pulse-labeled with 250 μM CldU for 30 min. For nascent strand degradation analysis, HeLa cells were sequentially pulse-labeled with 50 μM IdU and 250 μM CldU for 30 min and then treated with 4 mM HU for 5 h. Labeled cells were then trypsinized and resuspended in ice-cold PBS at 1 × 10^6 cells/ml. 2.5 μl of this resuspension were spotted onto a precleaned glass slide and lysed with 7.5 μl of lysis buffer (0.5% SDS, 50 mM EDTA, 200 mM Tris–HCl [pH 7.4]). 5 min later, the slides were tilted at 15° relative to horizontal, and the resulting DNA spreads were air-dried, fixed in methanol and acetic acid (3:1) for 20 min. The

DNA fibers were denatured with 3 M HCl overnight at 4°C, washed with PBS, and blocked with 1% BSA in PBS for 30 min at room temperature. Mouse anti-IdU/BrdU (BD Biosciences, clone B44, 1:500) and rat anti-CldU/BrdU (Abcam, ab2326, 1:500) antibodies were then applied to detect IdU and CldU, respectively. After a 3 h incubation, slides were washed with PBS and stained with Rhodamine-conjugated goat anti-mouse IgG (Jackson immunoresearch Laboratories, 1:500) and Alexan Fluor 488 Donkey anti Rat IgG (Life technologies, 1:500). Replication tracks were imaged on a Nikon Eclipse 80i Microscope equipped with a Plan Fluor 60× oil objective (NA 0.5–1.25; Nikon) and analyzed with NIS-Elements basic research imaging software (Nikon). The DNA tract lengths were measured using ImageJ software.

Electron microscopy

DNA analysis by electron microscopy was performed as previously described (41), with some modifications. Briefly, HeLa cells were treated with 4 mM HU for 3 h. Cells were then collected, resuspended in ice-cold PBS, and cross-linked by incubating with 10 μg/ml TMP (4,5′,8-trimethylpsoralen, Sigma-Aldrich) for 5 min in the dark, followed by a 3-min exposure to 365 nm UV light (BLE-7600B, Spectroline). The cycle of TMP addition, dark incubation, and irradiation was repeated 5 times. Cells were lysed with lysis buffer (1.28 M sucrose, 40 mM Tris–HCl [pH 7.5], 20 mM $MgCl_2$, and 4% Triton X-100) for 10 min at 4°C and digested with digestion buffer (800 mM guanidine–HCl, 30 mM Tris–HCl [pH 8.0], 30 mM EDTA [pH 8.0], 5% Tween-20, 0.5% Triton X-100, and 0.8 mg/ml proteinase K) for 2 h at 50°C. Genomic DNA was then extracted using chloroform/isoamylalcohol (24:1), purified by isopropanol precipitation, digested with PvuII HF restriction enzyme (New England Biolabs) for 3 h at 37°C, and concentrated using a QIAGEN-tip 20 column. Samples were prepared by spreading the concentrated DNA on a carbon-coated 400-mesh copper grid in the presence of benzyldimethylalkylammonium chloride, followed by platinum rotary shadowing using a High Vacuum Evaporator (MED 020, Leica). Images were obtained on a HT7700 transmission electron microscope equipped with a GATAN camera controlled by Digital Micrograph software.

In vivo ubiquitination and SUMOylation assays

HEK293T cells stably expressing His-tagged Ub/Ub-ΔGG or SUMO/SUMO-ΔGG were treated with or without 4 mM HU for 3 h. For the ubiquitination assay, cells were pretreated with 10 μM MG132 for 1 h before HU treatment. Cells were then collected, lysed, and sonicated in Buffer A (6 M guanidine–HCl, 100 mM NaH_2PO_4/Na_2HPO_4 and 15 mM imidazole). Clarified lysates were incubated with cobalt resin (Thermo Scientific) at 4°C overnight. The beads were then centrifuged and washed once with Buffer A, once with Buffer B (25 mM Tris–HCl [pH 6.8] and 10 mM imidazole). After washing, the resin-bound proteins were eluted by boiling in 2× SDS loading buffer supplemented with 250 mM imidazole and analyzed by SDS-PAGE. For the SUMOylation assay, cells were harvested and lysed in Buffer I (6 M guanidine–HCl, 100 mM NaH_2PO_4/Na_2HPO_4, 10 mM Tris–HCl [pH 8.0], and 5 mM imidazole). After sonication, the lysates were incubated with cobalt resin (Thermo Scientific) at 4°C overnight. Bound complexes were washed once each in Buffer I, Buffer II (8 M urea, 100 mM NaH_2PO_4/Na_2HPO_4 and 10 mM Tris–HCl [pH 8.0]), Buffer III (8 M urea, 100 mM NaH_2PO_4/Na_2HPO_4 and 10 mM Tris–HCl [pH 6.3]), and Buffer IV (25 mM Tris–HCl [pH 6.8] and 10 mM imidazole). The protein-bound beads were boiled in 2× SDS loading buffer supplemented with 250 mM imidazole and then subjected to SDS-PAGE.

Detection of chromosomal aberrations

HeLa cells were either mock-treated or treated with 4 mM HU for 3 h or 20 nM etoposide for 1 h. The cells were then incubated with colcemid (0.2 μg/ml) at 37°C for 4 h and were swollen using 75 mM KCl for 15 min at 37°C. After fixing in methanol/acetic acid (3:1) (vol/vol) for 20 min, cells were dropped onto ice-cold wet glass slides, air dried and stained with 5% Giemsa for 30 min. The average of two experiments is shown, at least 50 cells were counted in each experiment.

Recombinant protein purification

The coding sequences of wild-type and mutant RNF4 were cloned into pCold-GST expression vector and transformed into BL21 *E. coli* for expression of the GST-tagged fusion proteins. Cells were grown to mid-log phase and induced with 0.2 mM isopropyl β-D-1-thiogalactopyranoside (IPTG) at 16°C for 16 h. Cells were then collected, lysed, and sonicated in lysis buffer (20 mM Tris–HCl [pH 8.0], 300 mM NaCl, 1% Triton X-100, 2 mM DTT) containing protease inhibitors. Clarified lysates were incubated with glutathione–Sepharose resin (Thermo Scientific) for 4 h at 4°C. The beads were then centrifuged and washed three times with washing buffer A (20 mM Tris–HCl [pH 8.0], 500 mM NaCl, 0.5% NP-40, 2 mM DTT) containing protease inhibitors and once with washing buffer B (20 mM Tris–HCl [pH 8.0], 50 mM NaCl, 2 mM DTT) containing protease inhibitors. GST-tagged proteins were eluted with washing buffer B containing 20 mM reduced glutathione and subjected to dialysis prior to the *in vitro* ubiquitination assay. For the purification of GFP-tagged TOP2A or TOP2A-2KR, transfected HEK293T cells were lysed and sonicated in high-salt NETN buffer (20 mM Tris–HCl [pH 8.0], 500 mM NaCl, 1 mM EDTA and 0.5% Nonidet P-40). Clarified lysates were incubated with protein A–Sepharose coupled with the anti-GFP antibody for 3 h at 4°C. The beads were then centrifuged and washed three times with high-salt NETN buffer and twice with washing buffer B containing protease inhibitors. After washing, the resin-bound proteins were used to perform *in vitro* SUMOylation and ubiquitination assays. For the purification of Flag-tagged ZATT, transfected HEK293T cells were lysed and sonicated in high-salt NETN buffer containing protease inhibitors. Clarified lysates were incubated with protein A–Sepharose coupled with anti-Flag antibody for 3 h at 4°C. The beads were then centrifuged and washed three times with high-salt NETN buffer and twice with washing

buffer B. After washing, Flag-ZATT proteins was eluted with washing buffer B containing 0.2 mg/ml Flag peptide (GL Biochem Ltd).

In vitro SUMOylation assays

In vitro SUMOylation assays were carried out using a SUMOylation kit (Abcam, ab139470) according to the manufacturer's protocol. Briefly, 200 nM GFP-TOP2A-WT-, or 2KR-bound beads were incubated for 1 h at 37°C with the indicated reaction mixture in a total volume of 20 μl. The beads were then centrifuged and washed with washing buffer (20 mM Tris–HCl [pH 8.0], 50 mM NaCl, 2 mM DTT and 1 μg/ml of leupeptin and aprotinin) containing 2 mM *N*-ethylmaleimide and boiled in SDS sample buffer or subjected to the *in vitro* ubiquitination assay.

In vitro ubiquitination assay

SUMOylated TOP2A were incubated with 50 μM Ub, 200 nM UBA1, 1 μM UBcH5c and 5 μM RNF4 (wild-type or mutant) in 20 μl reaction buffer (25 mM Tris–HCl [pH 8.0], 50 mM NaCl, 2 mM DTT, 2mM ATP, and 5mM $MgCl_2$) at 37°C for 40 min. The beads were then washed with washing buffer (20 mM Tris–HCl [pH 8.0], 50 mM NaCl, 2 mM DTT and 1 μg/ml of leupeptin and aprotinin) containing 2 mM *N*-ethylmaleimide and boiled in SDS sample buffer.

Mass spectrometry

The LC–MS/MS analysis was performed on an Easy-nLC system coupled to a Thermo Q-Exactive HF mass spectrometerDesalted peptides were resuspended in buffer A (0.1% formic acid, 1.9% acetonitrile, 98% H_2O) and analyzed by analytical column (150 mm × 15 cm, 1.9 mm C18). Peptidess were separated with a 60 min linear gradient at flow rate 600 nl min^{-1} as follows: 6–15% buffer B (0.1% formic acid, 99.9% acetonitrile) for 16 min, 15–26% buffer B for 35 min, 26–42% buffer B for 15 min, 42–95% buffer B for 1 min, 95% B for 8 min. Peptides were measured by mass spectrometer in data-dependent mode with one full MS scan at $R = 120\,000$ (m/z 200), followed by twenty HCD MS/MS scans at $R = 15\,000$, NCE = 27, with an isolation width of 1.6 m/z. The AGC targets for MS1 and MS2 scans were 3 × 106 and 2 × 104, respectively, and the maximum injection time for MS1 and MS2 were 80 and 20 ms, respectively. Dynamic exclusion was set to 12 s. Precursors with unassigned charge states or charge states of 1+, >6+, were excluded. Data from Mass spectrometry were searched using MaxQuant (version 2.3). Human protein database was downloaded from NCBI (https://www.ncbi.nlm.nih.gov/). Tolerance of precursor ions and fragment ions were set to 10 ppm and 20 ppm, and maximum miscleavage sites was 2. For pull down experiments, variable modifications were Acetyl (Protein N-term), Oxidation (M). FDR of peptide lever and protein level were both 1%.

Cell survival assay

HeLa cells transfected with the indicated siRNAs were transferred into six-well plates at a density of 5 × 10^2 cells per well and incubated for 24 h before they were treated with HU or CPT at the indicated concentrations. Twenty-four hours later, the medium was replaced with fresh medium and cells were incubated for an additional 12 days. The resulting colonies were then fixed and stained with Coomassie blue.

Quantification and Statistical Analysis

Data are mean ± SEM from at least three independent experiments. Statistical significance of data was determined using one-way ANOVA. Significance is indicated by asterisk (****$P < 0.0001$; ***$P < 0.001$; **$P < 0.01$; *$P < 0.05$; ns, not significant) and $P < 0.05$ was considered statistically significant.

RESULTS

RNF4 forms a complex with TOP2A and ZATT

RNF4 plays important roles in many cellular processes, including DNA damage responses and gene transcription (27–29). RNF4 contains four functional SIM regions in its N terminus and a RING domain at its C-terminal region (Figure 1A). A previous study demonstrated that the catalytically-inactive mutant of RNF4 (RNF4-CS; substitution of cysteines 173 and 176 with serine residues) exhibited much more stable interactions with its substrates than its wild-type counterpart, and may be employed as a means to trap and identify novel RNF4 substrates (38). To isolate physiological substrates of RNF4, we utilized this 'substrate-trapping' approach in our tandem affinity purification-mass spectrometry (TAP-MS) experimentation. To this end we generated a HEK293T derivative cell line that stably expresses either a triple-epitope (SFB; S-protein, Flag, and streptavidin-binding peptide) tagged wild-type RNF4 or its 'substrate-trapping' mutant. Strikingly, two of the most highly-enriched interactors identified in RNF4-CS over wild-type RNF4 purifications were ZATT and TOP2A (Figure 1B, C, Supplementary Tables S1 and S2), both of which have been shown to cooperate with the DNA translocase PICH to drive extensive replication fork reversal in response to replication stress (9). Notably, ZATT and TOP2A have also been identified as RNF4 binding partners in several independent proteomic and biochemical studies (42,43).

To validate the TAP-MS results, we first carried out transient transfection and co-immunoprecipitation experiments. As shown in Figure 1D, the catalytically-inactive form of RNF4 interacted with ZATT and TOP2A more strongly than the active form. However, this difference was completely abolished by pre-treatment with the proteasome inhibitor MG132, indicating that RNF4 may target the TOP2A–ZATT protein complex for proteasomal degradation (Figure 1E). We further validated the interaction of RNF4 with the TOP2A–ZATT protein complex at endogenous levels (these experiments were performed in the presence of MG132 to prevent TOP2A and/or ZATT degradation) (Figure 1F). These findings, together with the observations that the RNF4–TOP2A/ZATT interactions were significantly stimulated by hydroxyurea (HU) treatment (Figure 1F) and TOP2A interacts with and is SUMOylated

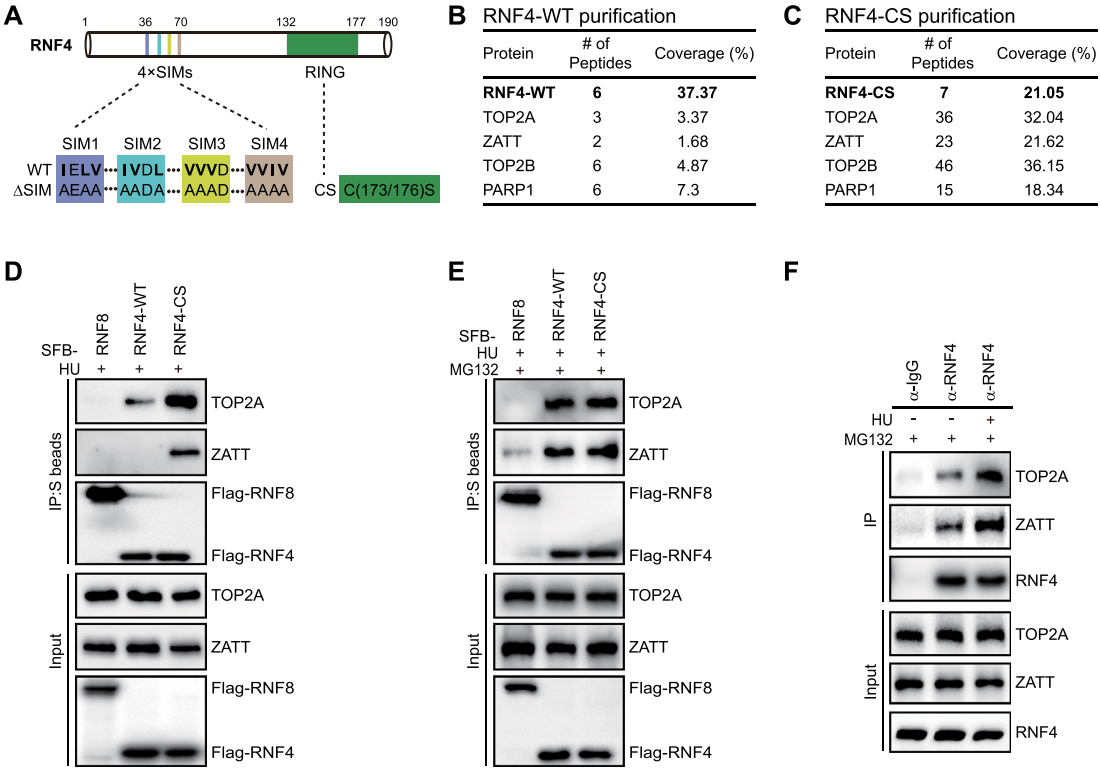

Protein	# of Peptides	Coverage (%)
RNF4-WT	**6**	**37.37**
TOP2A	3	3.37
ZATT	2	1.68
TOP2B	6	4.87
PARP1	6	7.3

Protein	# of Peptides	Coverage (%)
RNF4-CS	**7**	**21.05**
TOP2A	36	32.04
ZATT	23	21.62
TOP2B	46	36.15
PARP1	15	18.34

Figure 1. RNF4 forms a complex with TOP2A and ZATT. (**A**) Schematic illustration of RNF4 and its mutants used in this study. (**B**, **C**) List of proteins identified by mass spectrometry. Bait proteins are indicated in bold letters. HEK293T Cells stably expressing SFB-tagged wild-type RNF4 (RNF4-WT) or the catalytically- inactive mutant form of RNF4 (RNF4-CS) were treated with 4 mM HU for 3 h. Cells were then harvested and lysed with NETN buffer at 4°C for 30 min. Crude lysates were centrifuged at 4°C, 14 000 rpm for 10 min and the resulting supernatants were incubated with streptavidin-conjugated beads at 4°C for 3 h. Beads were washed three times with NETN buffer, and bounded proteins were eluted with NETN buffer containing 1 mg/ml biotin. Elutes were then incubated with S-protein beads at 4°C for 2 h. After washing three times with NETN buffer, the protein mixtures were subjected to mass spectrometry analysis. (**D**) HEK293T cells transiently transfected with plasmids encoding SFB-tagged RNF8, RNF4-WT, or RNF4-CS were treated with 4 mM HU for 3 h. Coprecipitation was carried out using S-protein beads, and immunoblotting was performed with the indicated antibodies. (**E**) HEK293T cells transiently transfected with plasmids encoding SFB-tagged RNF8, RNF4-WT or RNF4-CS were pre-treated with 10 μM MG132 for 1 h followed by treatment with 4 mM HU for 3 h. Coprecipitation was carried out using S-protein beads, and immunoblotting was performed with the indicated antibodies. (**F**) Association of endogenous RNF4 with TOP2A and ZATT. HeLa cells were pre-treated with 10 μM MG132 for 1 h followed by treatment with 4 mM HU for 3 h. Whole-cell lysates were immunoprecipitated with either anti-RNF4 antibodies or control IgG antibodies, followed by immunoblotting with anti-TOP2A, anti-ZATT and anti-RNF4 antibodies

by ZATT upon replication stress (9), suggest that SUMO-modified TOP2A may represent a *bona fide* substrate of RNF4.

RNF4 preferentially binds to SUMOylated TOP2A via its SIMs

It is now established that STUbLs preferentially recognize SUMOylated target proteins through its SIMs (27–29). To examine whether the SIMs of RNF4 may be required for its interaction with SUMO-modified TOP2A, we disrupted them in wild-type RNF4 (RNF4-ΔSIM) with point mutations (Figure 1A). Consistently, the resulting RNF4-ΔSIM mutant failed to interact with either endogenous TOP2A or ZATT in cells (Supplementary Figure S1A), indicating that the SIMs may mediate the RNF4 interaction with the TOP2A–ZATT protein complex. Moreover, and in line with the notion that ZATT facilitates TOP2A SUMOylation in response to replication stress (9), overexpression of wild-type ZATT, but not its enzymatic inactive mutant (ZATT-ΔSIM), significantly enhanced the RNF4–TOP2A interaction (Supplementary Figure S1B). More importantly, mutation of the two highly-conserved lysine residues (K1228K1240 to arginine; TOP2A-2KR) on the TOP2A polypeptide, which compromises TOP2A SUMOylation, markedly suppressed the replication stress-induced RNF4–TOP2A interaction (Supplementary Figure S1B). These results suggest that the RNF4–TOP2A interaction is mediated by SIMs, and requires TOP2A SUMOylation at lysines 1228 and 1240. In support of this conclusion, depletion of either UBC9, the sole SUMO-conjugating enzyme in mammalian cells, or the SUMO E3 ligase ZATT, greatly diminished RNF4–TOP2A interaction (Supplementary Figure S1C, D).

RNF4 accumulates at stalled replication forks following replication stress

Both TOP2A and ZATT are able to accumulate at stalled replication forks to drive extensive replication fork reversal upon replication stress (9). Given that RNF4 forms a complex with TOP2A and ZATT, we utilized the isolation of proteins on nascent DNA (iPOND) assay (Figure 2A) to test whether RNF4, like TOP2A and ZATT, can also be

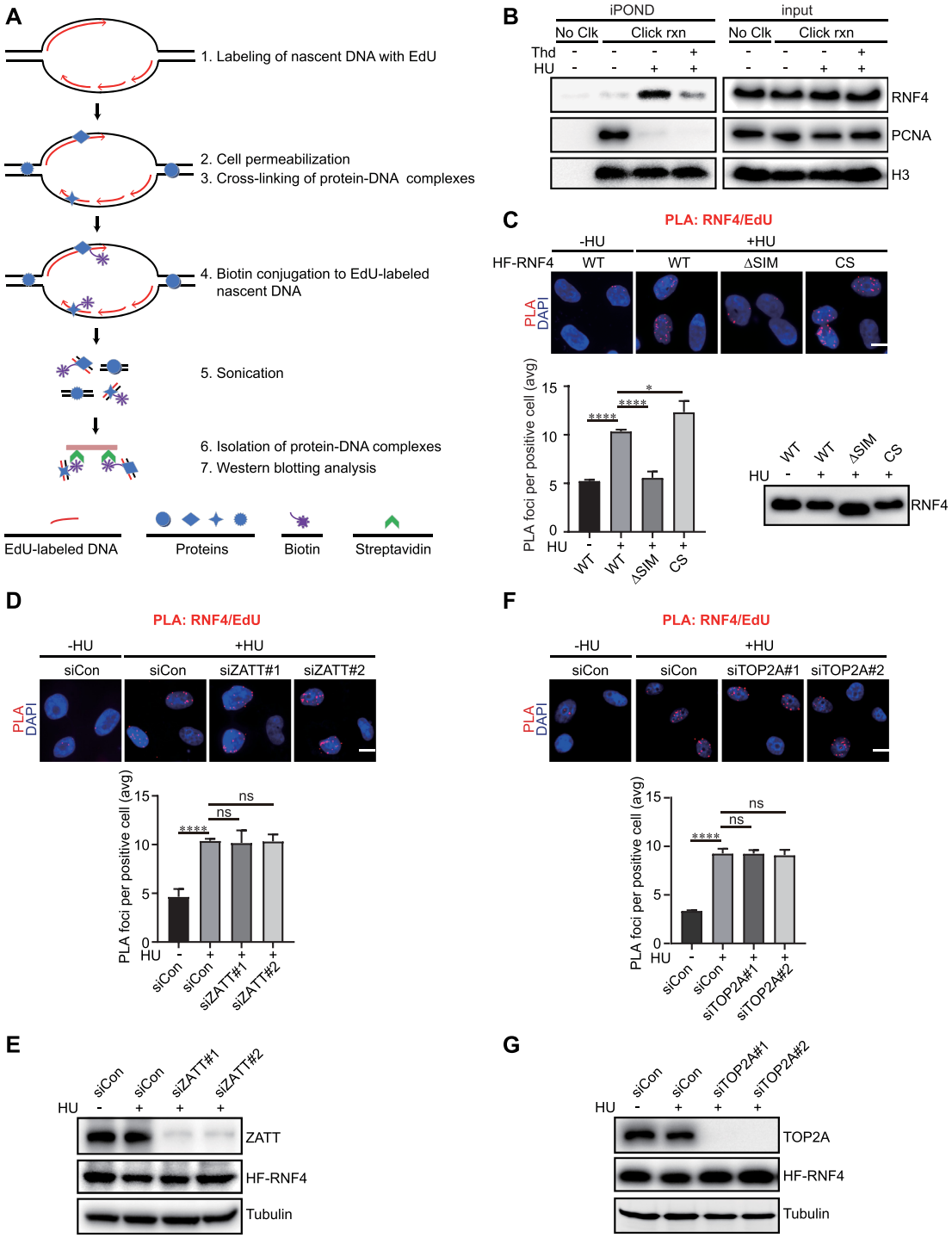

Figure 2. RNF4 accumulates at stalled replication forks in a SIM-dependent manner. (**A**) Schematic illustration of the iPOND assay. (**B**) Western blot analysis of the input and iPOND samples with the indicated antibodies. HEK293T cells were pulse-labeled with 10 μM EdU for 15 min followed with or without 10 μM thymidine chase for 1 h (Thd). Cells were then treated with 4 mM HU for 3 h prior to crosslinking with 1% formaldehyde. No Clk, no-click samples; Click rxn, Click reaction. (**C**) Analysis of RNF4 recruitment by PLA. HeLa cells stably expressing HF-tagged wild-type RNF4 or its mutants were pulse-labeled with 10 μM EdU for 15 min, left untreated or treated with 4 mM HU for 3 h, and then subjected to PLA with anti-Flag and anti-biotin antibodies. TOP: representative images of PLA foci. Scale bar, 10 μm. Bottom left: quantification of PLA foci number per focus positive cell. Data are means ± SEM of three independent experiments. At least 300 cells were counted in each individual experiment. $*P < 0.05$, $****P < 0.0001$, one-way ANOVA test. Bottom right: western blot analysis of RNF4 expression. (D, F) Depletion of ZATT (**D**) or TOP2A (**F**) does not affect RNF4 recruitment to stalled forks. HeLa cells stably expressing HF-tagged wild-type RNF4 were transfected with the indicated siRNAs, pulse-labeled with 10 μM EdU for 15 min, left untreated or treated with 4 mM HU for 3 h, and then subjected to PLA with anti-Flag and anti-biotin antibodies. Top: representative images of PLA foci. Scale bar, 10 μm. Bottom: quantification of PLA foci number per focus positive cell. Data are means ± SEM of three independent experiments. At least 300 cells were counted in each individual experiment. ns, not significant; $****P < 0.0001$, one-way ANOVA test. (E, G) Knockdown efficiency of ZATT (**E**) or TOP2A (**G**) was confirmed by Western blotting.

recruited to stalled replication forks. As shown in Figure 2B, PCNA was largely absent from stalled replication forks, as reported previously (44). Interestingly, RNF4 was highly enriched on nascent DNA but not on mature DNA (with a thymidine chase for 1 h) after HU treatment (Figure 2B). To further confirm the binding of RNF4 with nascent DNA, we performed the in-situ proximity ligation assay (PLA). Since our home-made RNF4 antibody is not suitable for immunostaining experiments, we generated a HeLa cell line that stably expresses HA-Flag-tagged RNF4 (HF-RNF4). As shown in Figure 2C, cells treated with HU displayed a dramatic increase in the number of RNF4/biotin PLA foci. Similar results were obtained following treatment with a sublethal dose of the topoisomerase II inhibitor etoposide (ETP) (Supplementary Figure S2A, B). These findings together suggest that RNF4 is recruited to stalled replication forks following replication stress.

We next investigated which domain on the RNF4 protein is required for its recruitment to stalled forks. As shown in Figure 2C, whereas wild-type RNF4 efficiently accumulated at stalled forks, the mutant lacking the SIMs failed to do so, suggesting that the SIMs are necessary for RNF4 accumulation at replication forks in response to replication stress. Interestingly, relative to wild-type RNF4, the catalytic-inactive mutant showed a slight increase in its ability to form PLA foci following replication stress (Figure 2C), indicating that RNF4 may associate with a SUMOylated substrate at stalled forks, and that inhibition of its activity may prolong the enzyme-substrate interaction, hence resulting in the increased PLA foci formation. Moreover, overexpression of SUMO2 or treatment with MG132 caused a significant increase in the number of RNF4/biotin PLA foci (Supplementary Figure S2C–F). These results, together with the observation that RNF4 interacts with the TOP2A–ZATT protein complex via its N-terminal SIMs, raise the possibility that SUMOylated TOP2A might be required for RNF4 recruitment to stalled forks. Surprisingly, depletion of TOP2A or ZATT did not notably affect replication stress-induced RNF4 PLA focus formation (Figure 2D–G and Supplementary Figure S2A-S2B). Given that RNF4 interacts with a variety of SUMO-modified proteins involved in DNA damage and replication stress responses, such as CtIP, MDC1, RPA and FANCD2/FANCI, it remains formally possible that RNF4 may be recruited to stalled forks through multiple protein-protein interactions.

RNF4 facilitates TOP2A ubiquitination and subsequent degradation

Given that STUbLs recognize SUMOylated proteins and catalyze their ubiquitination and degradation, we speculated that RNF4 might be able to promote SUMOylated TOP2A ubiquitination. Endogenous TOP2A was immunoprecipitated from HEK293T cells in the presence of NEM, a cysteine protease inhibitor that allows preservation of ubiquitinated cellular proteins, and then blotted with anti-ubiquitin antibodies. As shown in Supplementary Figure S3A, TOP2A ubiquitination was greatly enhanced following HU treatment. In addition, overexpression of wide-type SUMO2, but not the conjugation-deficient SUMO2-ΔGG mutant, resulted in a marked increase in TOP2A ubiquitination (Figure 3A). Significantly, the HU-induced SUMOylation-dependent ubiquitination of TOP2A was dramatically decreased when ZATT was depleted (Figure 3B and Supplementary Figure S3A). To further investigate the relationship between ubiquitination and SUMOylation of TOP2A, we used a non-SUMOylatable TOP2A-2KR allele, which contains two mutations that block TOP2A SUMOylation. As shown in Figure 3C, these mutations robustly suppressed TOP2A ubiquitination, suggesting that replication stress-induced ZATT-mediated SUMOylation of TOP2A is a prerequisite for its ubiquitination. A role of SUMOylation in stimulating TOP2A ubiquitination was further supported by the observation that UBC9 inactivation largely abolished HU-induced TOP2A ubiquitination (Figure 3B). Interestingly, downregulation of endogenous RNF4 in cells also significantly suppressed HU-induced SUMOylation-dependent TOP2A ubiquitination (Figure 3B and Supplementary Figure S3A), indicating that SUMOylated TOP2A is recognized and ubiquitinated by RNF4.

To further verify and to extend the above observations, we carried out *in vitro* SUMOylation assays followed by *in vitro* ubiquitination assays (Figure 3D). Interestingly, GFP-tagged TOP2A purified under high salt conditions was efficiently SUMOylated by ZATT *in vitro*, and was ubiquitinated by wild-type RNF4, but not its enzymatically-inactive mutant RNF4-CS (Figure 3E). In addition, mutation of the SIM consensus sequences on RNF4 greatly reduced its ability to ubiquitinate SUMOylated TOP2A *in vitro* (Figure 3E). More importantly, the SUMOylation-defective mutant TOP2A-2KR was also unable to be ubiquitinated by RNF4 (Figure 3E). Taken together, these results suggest that TOP2A is ubiquitinated by RNF4 in a SUMOylation-dependent manner.

Next, ubiquitinated TOP2A was analyzed by mass spectrometry (Supplementary Table S3) and databases (PhosphoSitePlus, mUbiSiDa) were mined to identify the putative ubiquitination sites on TOP2A. Based on these analysis, 98 lysine residues were predicted as putative ubiquitination sites. Strikingly, ubiquitination of TOP2A was largely blocked if the 20 high-probability ubiquitination sites were simultaneously mutated to arginine (TOP2A-20KR) (Supplementary Figure S3B-S3C).

To determine the physiological function of RNF4-mediated TOP2A ubiquitination, we measured the levels of SUMOylated TOP2A in RNF4-depleted or control cells. As shown in Figure 3F and Supplementary Figure S3D, knockdown of RNF4 resulted in a significant increase in the levels of SUMOylated TOP2A. Consistently, RNF4 depletion extended the half-life of SUMOylated TOP2A (Supplementary Figure S3E), suggesting that SUMOylated TOP2A is targeted by RNF4 for ubiquitination and subsequent degradation.

RNF4 limits excessive accumulation of the ZATT–TOP2A–PICH protein complex at stalled forks and controls the extent of fork reversal

The observations described above led us to hypothesize that RNF4-triggered ubiquitination and subsequent degradation of SUMOylated TOP2A might prevent excessive

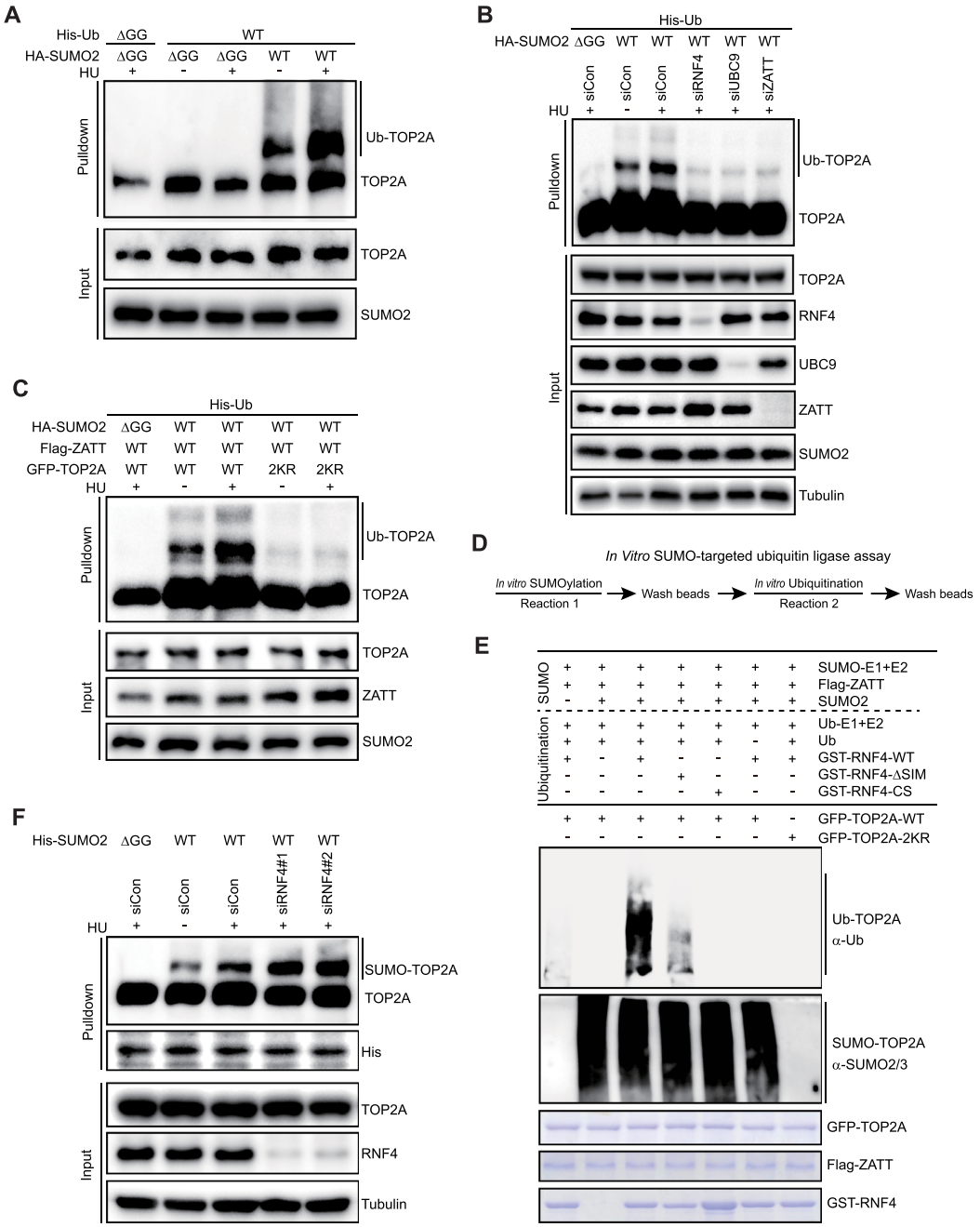

Figure 3. RNF4 targets SUMOylated TOP2A for ubiquitination and degradation. (**A**) SUMOylation of TOP2A stimulates its ubiquitination. HEK293T cells stably expressing His-tagged wild-type ubiquitin or the ΔGG mutant were transfected with HA-tagged wild-type SUMO2 or the ΔGG mutant. 24 h post-transfection, the cells were pre-treated with 10 μM MG132 for 1 h followed by treatment with or without 4 mM HU for 3 h. The cells were then harvested and lysed under denaturing conditions, and ubiquitinated proteins were purified by cobalt agarose resin. The isolated proteins were analyzed by Western blotting with the indicated antibodies. (**B**) RNF4, Ubc9, or ZATT depletion inhibits HU-induced TOP2A ubiquitination. HEK293T cells stably expressing His-tagged ubiquitin were transfected with the indicated plasmids/siRNAs. 24 h post-transfection, the cells were pre-treated with 10 μM MG132 for 1 h followed by treatment with or without 4 mM HU for 3 h. The cells were then harvested and lysed under denaturing conditions, and ubiquitinated proteins were purified by cobalt agarose resin. The isolated proteins were analyzed by Western blotting with the indicated antibodies. (**C**) Mutation of the SUMOylation sites of TOP2A impairs its ubiquitination. HEK293T cells stably expressing His-tagged ubiquitin were transfected with the indicated plasmids. 24 h post-transfection, the cells were pre-treated with 10 μM MG132 for 1 h followed by treatment with or without 4 mM HU for 3 h. The cells were then harvested and lysed under denaturing conditions, and ubiquitinated proteins were purified by cobalt agarose resin. The resulting isolated proteins were analyzed by Western blotting with the indicated antibodies. (**D**) Schematic illustration of the combined *in vitro* SUMOylation and ubiquitination assay procedures. (**E**) RNF4 ubiquitinates SUMOylated TOP2A *in vitro*. High-salt-purified GFP-TOP2A proteins were subjected to *in vitro* SUMOylation assays and then subjected to *in vitro* ubiquitination assays in the presence of bacterially expressed GST-RNF4-WT, GST-RNF4-ΔSIM, or GST-RNF4-CS, as indicated. The ubiquitination and SUMOylation of TOP2A were analyzed by Western blotting with the indicated antibodies. (**F**) RNF4 depletion increases the levels of SUMOylated TOP2A. HEK293T cells stably expressing His-tagged wild-type SUMO2 or the ΔGG mutant were transfected with the indicated siRNAs, followed by treatment with or without 4 mM HU for 3 h. The cells were then harvested and lysed under denaturing conditions, and SUMOylated TOP2A were purified by cobalt agarose resin. Immunoblotting was performed with the indicated antibodies.

accumulation of the ZATT–TOP2A–PICH protein complex at stalled replication forks. To test this hypothesis, we performed PLA to detect the association of the ZATT–TOP2A–PICH protein complex with biotin-labeled nascent DNA. As shown in Figure 4A, B and Supplementary Figure S4A-S4B, knockdown of RNF4 or treatment with MG132 resulted in a significant increase in the number of HU-induced TOP2A/biotin PLA foci. Strikingly, depletion of RNF4 did not potentiate the effect of MG132 treatment on TOP2A/biotin PLA foci formation (Supplementary Figure S4A, B). More importantly, ZATT as well as PICH also accumulated to supra-physiological levels at stalled forks in RNF4-depleted cells (Supplementary Figure S4C–F). These results, combined with the observations that the phenotypes observed in RNF4-depleted cells were reversed by re-expression of small interfering RNA (siRNA)-resistant wild-type RNF4 but not by either its ΔSIM mutant or its catalytically-inactive mutant (Figure 4A, B and Supplementary Figure S4C–F), suggest that RNF4 may regulate the turnover of the ZATT–TOP2A–PICH complex and hence its activity at stalled forks. Notably, knockdown of RNF4 in ZATT-depleted cells did not cause any increase in the number of TOP2A/biotin PLA foci (Supplementary Figure S4G, H). In line with this, RNF4 depletion did not obviously affect TOP2A-2KR/biotin PLA focus formation (Supplementary Figure S4I, J), reinforcing the idea that prior SUMOylation of TOP2A is required for its ubiquitination by RNF4.

Following replication stress, the ZATT–TOP2A–PICH protein complex drives extensive fork reversal to suppress unscheduled fork restart, thereby protecting stalled forks from collapse (9). Given that knockdown of RNF4 causes supra-physiological accumulation of the ZATT–TOP2A–PICH protein complex at stalled forks, we speculated that RNF4 may play a critical role in regulating the extent of fork reversal. To test this hypothesis, we measured the length of the regressed arms at reversed forks in wild-type and RNF4-depleted cells using an established electron microscopy approach. As shown in Figure 4C, D and Supplementary Figure S5A, downregulation of RNF4 caused a marked increase in the average length of regressed arms. In accordance with these findings, disruption of TOP2A ubiquitination also significantly increased the regressed arm length (Supplementary Figure S5B, C). More importantly, partial knockdown of TOP2A, ZATT or PICH largely suppressed the observed defect induced by RNF4 depletion (Supplementary Figure S5D, E). These results suggest that RNF4 may suppress excessive fork reversal by limiting activated ZATT–TOP2A–PICH complex dosage at stalled forks. Surprisingly, RNF4 depletion also led to a mild reduction in the frequency of reversed forks following HU treatment (Figure 4E).

Previous studies have shown that excessive fork reversal can result in uncontrolled degradation of nascent DNA at stalled replication forks (24–26). We thus performed the DNA fiber assay to test whether RNF4 is able to protect nascent DNA from degradation by suppressing excessive fork reversal. In this assay, cells were sequentially pulse-labeled with iododeoxyuridine (IdU) and chlorodeoxyuridine (CldU) for 30 min and then treated with HU for 5 h. Similar to BRCA1/2 depletion, RNF4 depletion also caused a reduced IdU:CldU ratio after treatment with HU (Figure 5A–C and Supplementary Figure S5F–H). Strikingly, knockdown of TOP2A efficiently prevented nascent DNA degradation caused by RNF4 inactivation following HU treatment (Figure 5D-F). Moreover, knockdown of RNF4 enhanced BRCA1/2 loss-induced stalled replication fork degradation (Figure 5A–C and Supplementary Figure S5F–H). Importantly, the increased levels of stalled replication fork degradation caused by RNF4 depletion could be largely suppressed by partial knockdown of TOP2A or PICH (Figure 5G–L). Taken together, these results suggest that RNF4 prevents excessive fork reversal and protects stalled forks from unscheduled degradation.

Loss of RNF4 impairs fork recovery and fork stability

We next asked whether excessive fork reversal observed in RNF4-depleted cells may affect replication fork restart upon cell recovery from replication stress. To this end, we performed the DNA fiber assay, in which cells were first pulse-labeled with IdU, incubated with HU or ETP to stall replication forks, and were then released into media containing CldU. As shown in Figure 6A, B and Supplementary Figure S6A, B, depletion of RNF4 led to a dramatic decrease in the ratio of CldU to IdU track lengths, indicating that RNF4 inactivation hampered restart of stalled forks.

Timely restart of stalled replication forks is essential for maintenance of fork stability. We thus examined whether RNF4 may be involved in the protection of stalled forks, by quantifying the symmetry of sister replication forks that initiate from the same replication origin. As shown in Figure 6C, D, RNF4 depletion resulted in a substantial increase in asymmetric sister forks, indicating increased frequencies of replication fork stalling or collapse. In support of this notion, RNF4-depleted cells had higher number of 53BP1 foci (a marker of DNA double-strand breaks) and displayed an increased frequency of chromosomal aberrations compared to control cells (Figure 6E–H and Supplementary Figure S6C–G). In addition, depletion of RNF4 rendered cells more sensitive to HU and CPT (Supplementary Figure S6H-S6I). The defects in replication restart and fork stability associated with RNF4 deficiency could be reversed by re-expression of siRNA-resistant wild-type RNF4, or by partial knockdown of TOP2A, ZATT or PICH, but not by re-expression of either its ΔSIM mutant or its enzymatic-inactivation mutant (Figure 6A–L). More importantly, the effect of partial TOP2A knockdown in suppressing these aberrant events observed in RNF4-depleted cells could be largely rescued by re-expression of siRNA-resistant wild-type TOP2A but not the SUMOylation-deficient mutant (Supplementary Figure S6J–N). Taken together, these results suggest that RNF4 controls the extent of fork reversal to preserve fork stability, and that this is effected by fine-tuning the activity of the ZATT–TOP2A–PICH protein complex at stalled replication forks.

DISCUSSION

Timely degradation of key regulatory proteins is of vital importance in the regulation of diverse cellular processes such

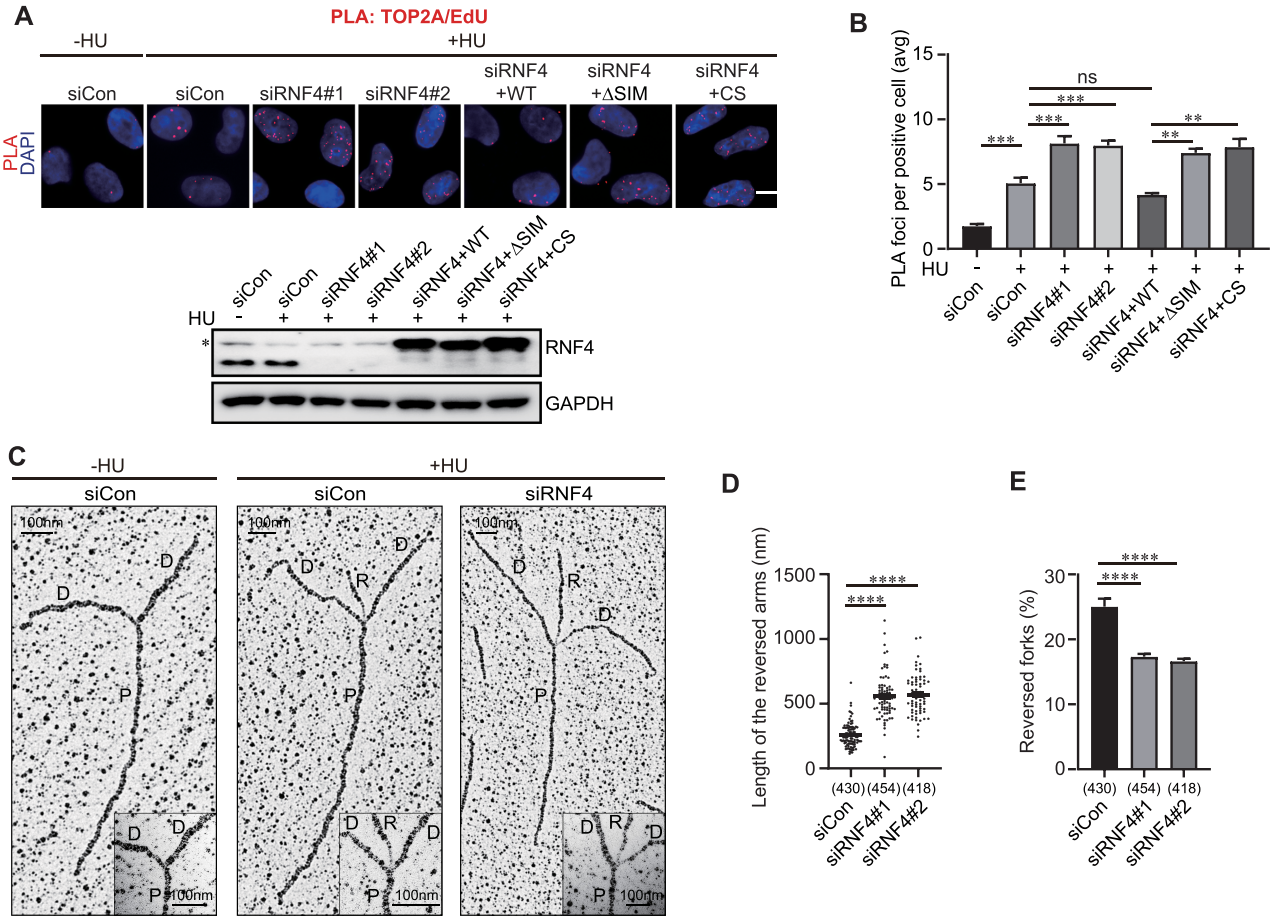

Figure 4. RNF4 depletion causes aberrant accumulation of the ZATT–TOP2A–PICH complex at stalled forks and excessive fork reversal. (**A**) RNF4 depletion increases the numbers of TOP2A/biotin PLA foci. HeLa cells transfected with the indicated siRNAs/plasmids were pulse-labeled with 10 μM EdU for 15 min, left untreated or treated with 4 mM HU for 3 h, and then subjected to PLA with anti-TOP2A and anti-biotin antibodies. Top: Representative images of PLA foci are shown. Scale bar, 10 μm. Bottom: Western blot analysis of RNF4 expression. The asterisk indicates a non-specific band. (**B**) Quantification of PLA foci number per focus positive cell. Data are means ± SEM of three independent experiments. At least 300 cells were counted in each individual experiment. ns, not significant; $^{**}P < 0.01$, $^{***}P < 0.001$, one-way ANOVA test. (**C**) Representative electron microscopy images of reversed forks in wild-type or RNF4-depleted HeLa cells. P, Parental strand; D, Daughter strand; R, Regressed arm. (**D**) Dot plot of the regressed arm length in cells transfected with the indicated siRNAs. Data represent at least three independent experiments. In brackets, the number of analyzed replication intermediates is shown. $^{****}P < 0.0001$, one-way ANOVA test. (**E**) Frequency of reversed forks in wild-type or RNF4-depleted HeLa cells treated with 4 mM HU for 3 h. Data are means ± SEM of three independent experiments. In brackets, the number of analyzed replication intermediates is shown. $^{****}P < 0.0001$, one-way ANOVA test.

as DNA damage repair, cell cycle control, and gene transcription. STUbLs play important roles in the maintenance of genome integrity by regulating the stability of a subset of SUMOylated proteins (27–29,45–47). To date, only a few STUBLs have been identified, including Slx5-Slx8 in budding yeast, Rfp1-2/Slx8 in fission yeast, and RNF4 and RNF111/Arkadia in mammalian cells (27–29,45–47). Previous studies by others and ourselves have uncovered important regulatory roles of the mammalian STUbLs RNF4 and RNF111/Arkadia in facilitating the extraction of a series of DNA damage response proteins, including CtIP, MDC1, FANCD2/FANCI, RPA, BRCA1 and XPC, from sites of DNA damage (35–39,45–47). However, whether these STUBLs also have crucial roles in protecting stalled replication forks is not clearly defined. In the current study, we uncovered a novel role for the mammalian STUbL RNF4 in fine-tuning the activity of the ZATT–TOP2A–PICH complex at stalled replication forks, and in regulating the extent of replication fork reversal. Mechanistically, RNF4 interacts with SUMOylated TOP2A and that this interaction is increased in response to replication stress, resulting in TOP2A poly-ubiquitination and subsequent proteasomal degradation. Based on the previous studies and the data presented here, we would like to propose a revised model for replication fork reversal (Figure 7). Briefly, upon replication stress, DNA translocases, such as SMARCAL1/HARP, ZRANB3 and HLTF, cooperate with the RAD51 recombinase to initiate limited fork reversal, generating positive torsional stress in the newly replicated sister chromatids. TOP2A then recognizes and relieves the resulting topological barriers, and at the same time, is SUMOylated by the SUMO E3 ligase ZATT. On one hand, SUMOylated TOP2A recruits the SUMO-targeted DNA translocase PICH to stalled fork to facilitate extensive fork reversal, which in turn would produce additional substrates for TOP2A, on the other hand, SUMOylated TOP2A is rec-

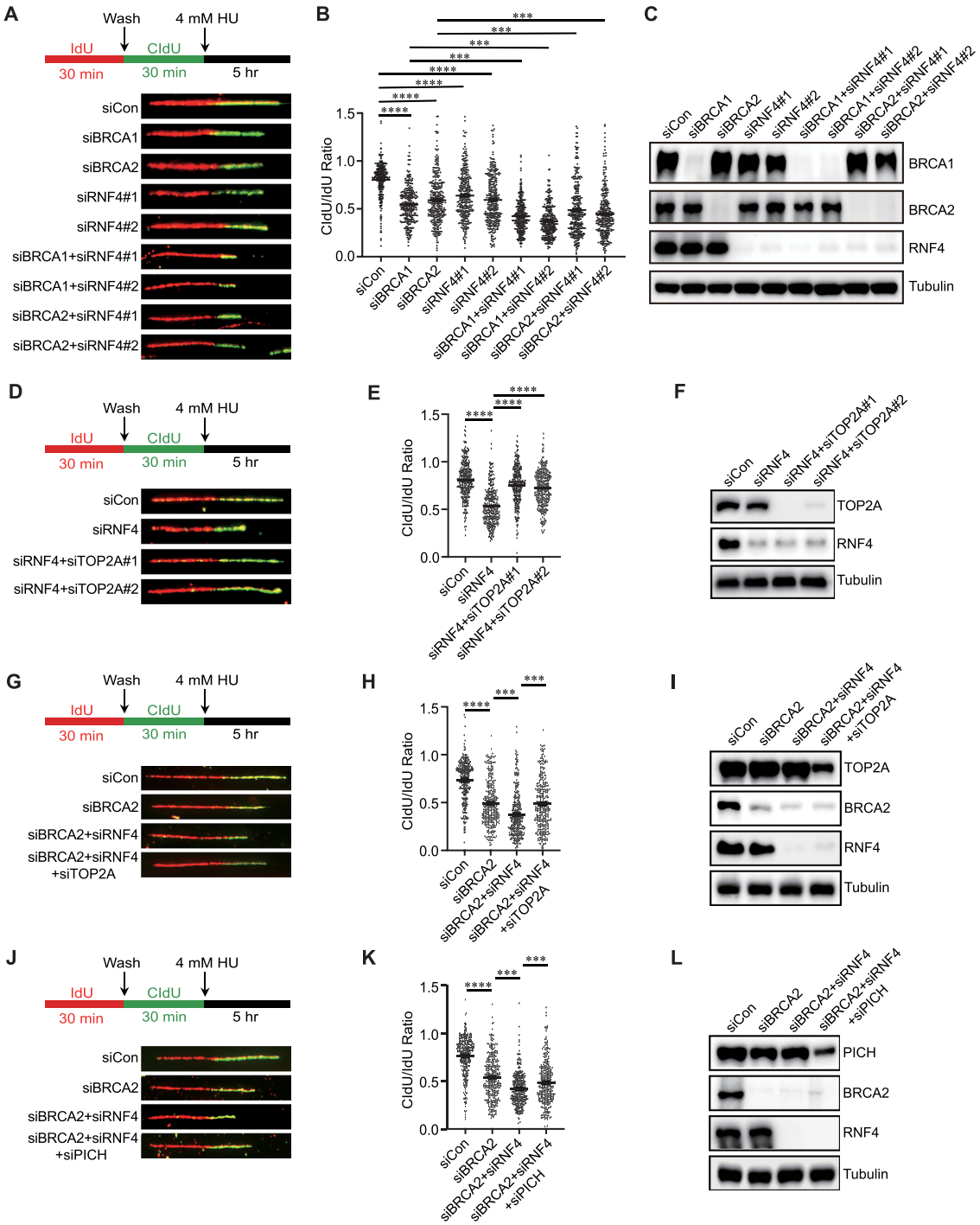

Figure 5. RNF4 protects stalled forks from unscheduled degradation. (**A**) RNF4 depletion causes degradation of nascent DNA at stalled forks. Top: schematic of DNA fibers experiment. HeLa cells transfected with the indicated siRNAs were sequentially pulse-labeled with IdU and CldU for 30 min and then treated with HU for 5 h. Bottom: representative IdU and CldU replication tracks in cells transfected with the indicated siRNAs. (**B**) Dot plot of CldU to IdU track length ratios for individual replication forks in cells transfected with the indicated siRNAs. Data are representative of at least three independent experiments. More than 300 fibers were measured for each sample. ***$P < 0.001$; ****$P < 0.0001$, one-way ANOVA test. (**C**) Knockdown efficiency of RNF4 and BRCA1/2 was confirmed by western blotting. (**D**) TOP2A depletion prevents nascent DNA degradation caused by RNF4 inactivation. Top: schematic of DNA fibers experiment. Bottom: representative IdU and CldU replication tracks in cells transfected with the indicated siRNAs. (**E**) Dot plot of CldU to IdU track length ratios for individual replication forks in cells transfected with the indicated siRNAs. Data are representative of at least three independent experiments. ****$P < 0.0001$, one-way ANOVA test. (**F**) Knockdown efficiency was confirmed by western blotting. (**G**, **J**) Top: schematic of DNA fibers experiment. HeLa cells transfected with the indicated siRNAs were sequentially pulse-labeled with IdU and CldU for 30 min and then treated with HU for 5 h. Bottom: representative IdU and CldU replication tracks in cells transfected with the indicated siRNAs. (**H**, **K**) Dot plot of CldU to IdU track length ratios for individual replication forks in cells transfected with the indicated siRNAs. Data are representative of at least three independent experiments. More than 300 fibers were measured for each sample. ***$P < 0.001$; ****$P < 0.0001$, one-way ANOVA test. (**I**, **L**) Knockdown efficiency was confirmed by western blotting.

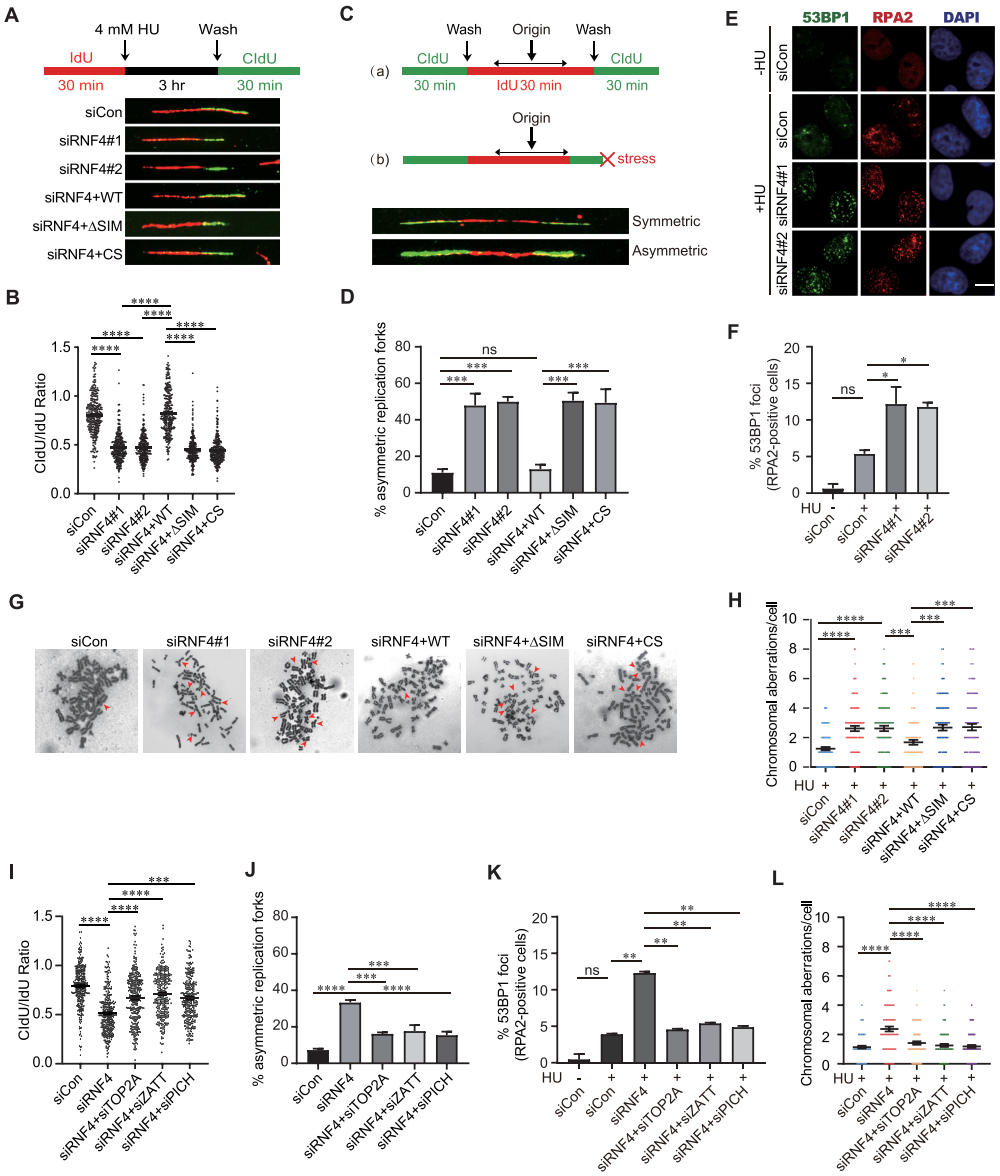

Figure 6. RNF4 maintains replication fork stability. (**A**) Top: schematic representation of the DNA fiber assay. HeLa cells transfected with the indicated siRNAs/plasmids were pulse-labeled with IdU for 30 min, treated with 4 mM HU for 3 h, and then subjected to a pulse-labeling with CldU for 30 min. Bottom: representative IdU and CldU replication tracks in cells transfected with the indicated siRNAs/plasmids. (**B**) Dot plot of CldU/IdU track length ratios for individual replication forks in cells transfected with the indicated siRNAs/plasmids. Data represent at least three independent experiments. At least 300 fibers were measured for each sample. $^{****}P < 0.0001$, one-way ANOVA test. (**C**) Top: schematic representation of the DNA fiber assay. Bottom: representative images of symmetric and asymmetric forks. (**D**) The percentages of asymmetric forks in wild-type or RNF4-depleted HeLa cells. For each replication origin, if a CldU tract length ratio is larger than 1.67 or smaller than 0.6, the fork was defined as asymmetric. Data are means ± SEM of three independent experiments. More than 150 fibers were measured for each sample. ns, not significant; $^{***}P < 0.001$, one-way ANOVA test. (**E**) Depletion of RNF4 causes fork collapse, resulting in DSB formation. HeLa cells transfected with the indicated siRNAs were left untreated or treated with 4 mM HU for 3 h. The cells were then processed for 53BP1 and RPA2 immunofluorescence. Representative 53BP1/RPA2 foci are shown. Scale bar, 10 μm. (**F**) Quantification of 53BP1 foci in RPA2-positive cells. Data are means ± SEM of three independent experiments. At least 300 cells were counted in each individual experiment. ns, not significant; $^{*}P < 0.05$, one-way ANOVA test. (**G-H**) Representative images of metaphase spreads prepared from control or RNF4-depleted HeLa cells treated with HU (4 mM for 3 h). Aberrations are marked by arrows (G). Quantification of chromosomal aberrations in control and RNF4-depleted HeLa cells (H). The average of two experiments is shown; at least 50 cells were counted in each experiment. $^{***}P < 0.001$; $^{****}P < 0.0001$, one-way ANOVA test. (**I**) Dot plot of CldU/IdU track length ratios for individual replication forks. HeLa cells transfected with the indicated siRNAs were pulse-labeled with IdU for 30 min, treated with 4 mM HU for 3 h, and then subjected to a pulse-labeling with CldU for 30 min. Data represent at least three independent experiments. At least 300 fibers were measured for each sample. $^{***}P < 0.001$; $^{****}P < 0.0001$, one-way ANOVA test. (**J**) The percentages of asymmetric forks in HeLa cells transfected with the indicated siRNAs. For each replication origin, if a CldU tract length ratio is larger than 1.67 or smaller than 0.6, the fork was defined as asymmetric. Data are means ± SEM of three independent experiments. More than 150 fibers were measured for each sample. $^{***}P < 0.001$; $^{****}P < 0.0001$, one-way ANOVA test. (**K**) Quantification of 53BP1 foci in RPA2-positive cells. HeLa cells transfected with the indicated siRNAs were left untreated or treated with 4 mM HU for 3 h. Data are means ± SEM of three independent experiments. At least 300 cells were counted in each individual experiment. ns, not significant; $^{**}P < 0.01$, one-way ANOVA test. (**L**) Quantification of chromosomal aberrations in HeLa cells transfected with the indicated siRNAs. The average of two experiments is shown; at least 50 cells were counted in each experiment. $^{****}P < 0.0001$, one-way ANOVA test.

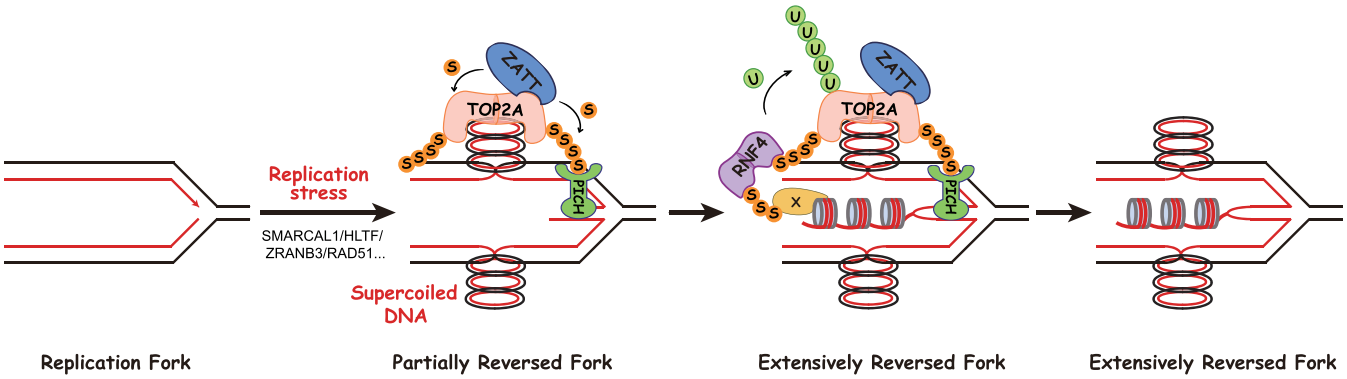

Figure 7. Working model depicting a proposed model of RNF4 in regulating replication fork reversal. X indicates as-yet-unidentified proteins that are important for RNF4 recruitment to stalled replication forks; S indicates SUMO; U indicates ubiquitin.

ognized and is poly-ubiquitinated by RNF4, thereby preventing excessive fork reversal. Our results suggest a dual role of TOP2A SUMOylation in regulating the extent of fork reversal: (i) by recruiting PICH to stalled forks to ensure efficient fork reversal and to suppress unscheduled restart, and (ii) by facilitating its interaction with RNF4 to suppress excessive fork reversal and to prevent stalled forks from collapsing.

The RNF4–TOP2A interaction is mediated by SIMs and requires ZATT-mediated TOP2A SUMOylation. However, RNF4 seems to interact with unmodified TOP2A, rather than a slower-migrating species which is indicative of the SUMOylated form (Figure 1D–F). One explanation is that SUMOylation is a very dynamic process and the activities of deSUMOylating enzymes cause a rapid loss of SUMO conjugates in most standard cell extracts. To inhibit the highly active SUMO protease and preserve SUMOylation, samples are normally lysed in denaturing conditions. In our co-immunoprecipitation experiments, cell extracts were prepared under non-denaturing conditions. Thus, conjugated SUMO might be removed from TOP2A by deSUMOylating enzymes during the process of the co-immunoprecipitation experiments. We speculate that the SIM–SUMO interaction may cause conformational changes in TOP2A, resulting in exposing additional binding sites for RNF4. Consequently, after binding to RNF4, even conjugated SUMO was removed from TOP2A, the RNF4–TOP2A interaction can still be detected (via additional binding sites). Future studies would be needed to test this possibility.

Consistent with a direct role of RNF4 in promoting SUMOylated TOP2A ubiquitination and degradation, its depletion resulted in aberrant accumulation of the ZATT–TOP2A–PICH protein complex at stalled replication forks, which in turn caused excessive fork reversal and increased frequency of fork collapse. Surprisingly, depletion of RNF4 also reduced the frequency of reversed forks following replication stress (Figure 4E). One possibility is that defective removal of the ZATT–TOP2A–PICH protein complex impairs its recycling efficiency and in turn results in a reduction in the frequency of reversed forks. Our findings suggest that timely removal of the ZATT–TOP2A–PICH protein complex from stalled forks is an important molecular event in the regulation of fork reversal, and further strengthen the idea that dynamic regulation of the replication stress response proteins at stalled replication forks is critical for proper cellular response to replication stress.

It is noteworthy to mention that while the levels of SUMOylated TOP2A were significantly increased in RNF4-depleted cells, the total protein levels of TOP2A were not detectably altered (Figure 3F). These findings are in line with previous observations wherein protein SUMOylation almost always occurs at very low stoichiometry (48), and consequently, subsequent poly-ubiquitination and degradation by RNF4 only affects a small fraction of its target substrates. Given that deregulation of TOP2A SUMOylation by depletion of RNF4 or depletion of the SUMO E3 ligase ZATT caused stalled fork instability, our results indicate that this small SUMOylated proportion of TOP2A is functionally very important and may represent the functionally-active fraction.

Similar to proteins involved in the cellular response to replication stress, RNF4 is also able to accumulate at stalled replication forks. Productive recruitment of RNF4 to stalled forks relies on its SIMs, but is independent of its RING domain (Figure 2C). In stark contrast, RNF4 is recruited to DNA damage sites in a manner dependent on both its SIMs and its RING domain, in addition to the upstream molecules NBS1, MDC1, RNF8, 53BP1 and BRCA1 (34–36). These results suggest that the mechanisms by which RNF4 is recruited to sites of DNA damage and to stalled replication forks are different. Surprisingly, although RNF4 bound to SUMOylated TOP2A in a SIM-dependent manner, depletion of TOP2A or ZATT did not affect RNF4 recruitment to stalled forks (Figure 2D–G and Supplementary Figure S2A, B). It is thus highly possible that multiple SUMOylated proteins at stalled forks simultaneously contribute to the recruitment of RNF4 to stalled forks and the underlying mechanisms warrant further investigation.

Unlike BRCA1/2, which maintain nascent replication tracts by stabilizing RAD51 nucleofilaments (49), RNF4 protects stalled forks from unscheduled degradation by preventing excessive fork reversal. In support of this notion, downregulation of RNF4 enhanced BRCA1/2 loss-induced stalled fork degradation. These findings raise the possibility that a synthetic lethality may arise when these two dif-

ferent fork protection mechanisms are compromised simultaneously. Thus, targeting RNF4 activities may offer new therapeutic opportunities for treating BRCA1/2-deficient tumors.

DATA AVAILABILITY

All data are available in the main text or the supplementary materials. Mass spectrometry data has been deposited to the ProteomeXchange consortium under dataset identifier PXD028397.

SUPPLEMENTARY DATA

Supplementary Data are available at NAR Online.

ACKNOWLEDGEMENTS

We thank the Life Sciences Institute core facilities, Zhejiang University for technical assistance. We are grateful to all members of the Huang group for helpful discussions.

FUNDING

National Natural Science Foundation of China [31961160725, 31730021, 31971220, 3170040161, 81970956, 32170730]; National Key Research and Development Program of China [2021YFA1101000 and 2018YFC2000100]; Fok Ying Tung Education Foundation; China's Fundamental Research Funds for the Central Universities. Funding for open access charge: National Natural Science Foundation of China [31961160725, 31730021, 31971220, 3170040161, 81970956, 32170730]; National Key Research and Development Program of China [2021YFA1101000 and 2018YFC2000100]; Fok Ying Tung Education Foundation; China's Fundamental Research Funds for the Central Universities.
Conflict of interest statement. None declared.

REFERENCES

1. Ciccia,A. and Elledge,S.J. (2010) The DNA damage response: making it safe to play with knives. *Mol. Cell*, **40**, 179–204.
2. Branzei,D. and Foiani,M. (2009) The checkpoint response to replication stress. *DNA Repair (Amst.)*, **8**, 1038–1046.
3. Huen,M.S. and Chen,J. (2010) Assembly of checkpoint and repair machineries at DNA damage sites. *Trends Biochem. Sci*, **35**, 101–108.
4. Berti,M., Cortez,D. and Lopes,M. (2020) The plasticity of DNA replication forks in response to clinically relevant genotoxic stress. *Nat. Rev. Mol. Cell Biol.*, **21**, 633–651.
5. Rickman,K. and Smogorzewska,A. (2019) Advances in understanding DNA processing and protection at stalled replication forks. *J. Cell Biol.*, **218**, 1096–1107.
6. Poole,L.A. and Cortez,D. (2017) Functions of SMARCAL1, ZRANB3, and HLTF in maintaining genome stability. *Crit. Rev. Biochem. Mol. Biol.*, **52**, 696–714.
7. Neelsen,K.J. and Lopes,M. (2015) Replication fork reversal in eukaryotes: from dead end to dynamic response. *Nat. Rev. Mol. Cell Biol.*, **16**, 207–220.
8. Quinet,A., Lemacon,D. and Vindigni,A. (2017) Replication fork reversal: players and guardians. *Mol. Cell*, **68**, 830–833.
9. Tian,T., Bu,M., Chen,X., Ding,L., Yang,Y., Han,J., Feng,X.H., Xu,P., Liu,T., Ying,S. *et al.* (2021) The ZATT–TOP2A–PICH axis drives extensive replication fork reversal to promote genome stability. *Mol. Cell*, **81**, 198–211.
10. Zellweger,R., Dalcher,D., Mutreja,K., Berti,M., Schmid,J.A., Herrador,R., Vindigni,A. and Lopes,M. (2015) Rad51-mediated replication fork reversal is a global response to genotoxic treatments in human cells. *J. Cell Biol.*, **208**, 563–579.
11. Betous,R., Mason,A.C., Rambo,R.P., Bansbach,C.E., Badu-Nkansah,A., Sirbu,B.M., Eichman,B.F. and Cortez,D. (2012) SMARCAL1 catalyzes fork regression and holliday junction migration to maintain genome stability during DNA replication. *Genes Dev.*, **26**, 151–162.
12. Ciccia,A., Nimonkar,A.V., Hu,Y., Hajdu,I., Achar,Y.J., Izhar,L., Petit,S.A., Adamson,B., Yoon,J.C., Kowalczykowski,S.C. *et al.* (2012) Polyubiquitinated PCNA recruits the ZRANB3 translocase to maintain genomic integrity after replication stress. *Mol. Cell*, **47**, 396–409.
13. Kile,A.C., Chavez,D.A., Bacal,J., Eldirany,S., Korzhnev,D.M., Bezsonova,I., Eichman,B.F. and Cimprich,K.A. (2015) HLTF's ancient HIRAN domain binds 3' DNA ends to drive replication fork reversal. *Mol. Cell*, **58**, 1090–1100.
14. Blastyak,A., Hajdu,I., Unk,I. and Haracska,L. (2010) Role of double-stranded DNA translocase activity of human HLTF in replication of damaged DNA. *Mol. Cell. Biol.*, **30**, 684–693.
15. Vujanovic,M., Krietsch,J., Raso,M.C., Terraneo,N., Zellweger,R., Schmid,J.A., Taglialatela,A., Huang,J.W., Holland,C.L., Zwicky,K. *et al.* (2017) Replication fork slowing and reversal upon DNA damage require PCNA polyubiquitination and ZRANB3 DNA translocase activity. *Mol. Cell*, **67**, 882–890.
16. Achar,Y.J., Balogh,D., Neculai,D., Juhasz,S., Morocz,M., Gali,H., Dhe-Paganon,S., Venclovas,C. and Haracska,L. (2015) Human HLTF mediates postreplication repair by its HIRAN domain-dependent replication fork remodelling. *Nucleic Acids Res.*, **43**, 10277–10291.
17. Bugreev,D.V., Rossi,M.J. and Mazin,A.V. (2011) Cooperation of RAD51 and RAD54 in regression of a model replication fork. *Nucleic Acids Res.*, **39**, 2153–2164.
18. Berti,M., Teloni,F., Mijic,S., Ursich,S., Fuchs,J., Palumbieri,M.D., Krietsch,J., Schmid,J.A., Garcin,E.B., Gon,S. *et al.* (2020) Sequential role of RAD51 paralog complexes in replication fork remodeling and restart. *Nat. Commun.*, **11**, 3531.
19. Gari,K., Decaillet,C., Delannoy,M., Wu,L. and Constantinou,A. (2008) Remodeling of DNA replication structures by the branch point translocase FANCM. *Proc. Natl. Acad. Sci. U.S.A.*, **105**, 16107–16112.
20. Fugger,K., Mistrik,M., Neelsen,K.J., Yao,Q., Zellweger,R., Kousholt,A.N., Haahr,P., Chu,W.K., Bartek,J., Lopes,M. *et al.* (2015) FBH1 catalyzes regression of stalled replication forks. *Cell Rep.*, **10**, 1749–1757.
21. Machwe,A., Xiao,L., Groden,J. and Orren,D.K. (2006) The werner and bloom syndrome proteins catalyze regression of a model replication fork. *Biochemistry*, **45**, 13939–13946.
22. Ralf,C., Hickson,I.D. and Wu,L. (2006) The bloom's syndrome helicase can promote the regression of a model replication fork. *J. Biol. Chem.*, **281**, 22839–22846.
23. Kanagaraj,R., Saydam,N., Garcia,P.L., Zheng,L. and Janscak,P. (2006) Human RECQ5beta helicase promotes strand exchange on synthetic DNA structures resembling a stalled replication fork. *Nucleic Acids Res.*, **34**, 5217–5231.
24. Malacaria,E., Pugliese,G.M., Honda,M., Marabitti,V., Aiello,F.A., Spies,M., Franchitto,A. and Pichierri,P. (2019) Rad52 prevents excessive replication fork reversal and protects from nascent strand degradation. *Nat. Commun.*, **10**, 1412.
25. Dungrawala,H., Bhat,K.P., Le Meur,R., Chazin,W.J., Ding,X., Sharan,S.K., Wessel,S.R., Sathe,A.A., Zhao,R. and Cortez,D. (2017) RADX promotes genome stability and modulates chemosensitivity by regulating RAD51 at replication forks. *Mol. Cell*, **67**, 374–386.
26. Couch,F.B., Bansbach,C.E., Driscoll,R., Luzwick,J.W., Glick,G.G., Betous,R., Carroll,C.M., Jung,S.Y., Qin,J., Cimprich,K.A. *et al.* (2013) ATR phosphorylates SMARCAL1 to prevent replication fork collapse. *Genes Dev.*, **27**, 1610–1623.
27. Prudden,J., Pebernard,S., Raffa,G., Slavin,D.A., Perry,J.J., Tainer,J.A., McGowan,C.H. and Boddy,M.N. (2007) SUMO-targeted ubiquitin ligases in genome stability. *EMBO J.*, **26**, 4089–4101.

28. Sun,H., Leverson,J.D. and Hunter,T. (2007) Conserved function of RNF4 family proteins in eukaryotes: targeting a ubiquitin ligase to SUMOylated proteins. *EMBO J.*, **26**, 4102–4112.
29. Sun,H. and Hunter,T. (2012) Poly-small ubiquitin-like modifier (PolySUMO)-binding proteins identified through a string search. *J. Biol. Chem.*, **287**, 42071–42083.
30. Lallemand-Breitenbach,V., Jeanne,M., Benhenda,S., Nasr,R., Lei,M., Peres,L., Zhou,J., Zhu,J., Raught,B. and de The,H. (2008) Arsenic degrades PML or PML-RARalpha through a SUMO-triggered RNF4/ubiquitin-mediated pathway. *Nat. Cell Biol.*, **10**, 547–555.
31. Tatham,M.H., Geoffroy,M.C., Shen,L., Plechanovova,A., Hattersley,N., Jaffray,E.G., Palvimo,J.J. and Hay,R.T. (2008) RNF4 is a poly-SUMO-specific E3 ubiquitin ligase required for arsenic-induced PML degradation. *Nat. Cell Biol.*, **10**, 538–546.
32. Liew,C.W., Sun,H., Hunter,T. and Day,C.L. (2010) RING domain dimerization is essential for RNF4 function. *Biochem. J.*, **431**, 23–29.
33. Plechanovova,A., Jaffray,E.G., McMahon,S.A., Johnson,K.A., Navratilova,I., Naismith,J.H. and Hay,R.T. (2011) Mechanism of ubiquitylation by dimeric RING ligase RNF4. *Nat. Struct. Mol. Biol.*, **18**, 1052–1059.
34. Luo,K., Zhang,H., Wang,L., Yuan,J. and Lou,Z. (2012) Sumoylation of MDC1 is important for proper DNA damage response. *EMBO J.*, **31**, 3008–3019.
35. Galanty,Y., Belotserkovskaya,R., Coates,J. and Jackson,S.P. (2012) RNF4, a SUMO-targeted ubiquitin E3 ligase, promotes DNA double-strand break repair. *Genes Dev.*, **26**, 1179–1195.
36. Yin,Y., Seifert,A., Chua,J.S., Maure,J.F., Golebiowski,F. and Hay,R.T. (2012) SUMO-targeted ubiquitin E3 ligase RNF4 is required for the response of human cells to DNA damage. *Genes Dev.*, **26**, 1196–1208.
37. Vyas,R., Kumar,R., Clermont,F., Helfricht,A., Kalev,P., Sotiropoulou,P., Hendriks,I.A., Radaelli,E., Hochepied,T., Blanpain,C. *et al.* (2013) RNF4 is required for DNA double-strand break repair in vivo. *Cell Death Differ.*, **20**, 490–502.
38. Gibbs-Seymour,I., Oka,Y., Rajendra,E., Weinert,B.T., Passmore,L.A., Patel,K.J., Olsen,J.V., Choudhary,C., Bekker-Jensen,S. and Mailand,N. (2015) Ubiquitin-SUMO circuitry controls activated fanconi anemia ID complex dosage in response to DNA damage. *Mol. Cell*, **57**, 150–164.
39. Han,J., Wan,L., Jiang,G., Cao,L., Xia,F., Tian,T., Zhu,X., Wu,M., Huen,M.S.Y., Wang,Y. *et al.* (2021) ATM controls the extent of DNA end resection by eliciting sequential posttranslational modifications of CtIP. *Proc. Natl. Acad. Sci. U.S.A.*, **118**, 22022600118.
40. Sirbu,B.M., Couch,F.B., Feigerle,J.T., Bhaskara,S., Hiebert,S.W. and Cortez,D. (2011) Analysis of protein dynamics at active, stalled, and collapsed replication forks. *Genes Dev.*, **25**, 1320–1327.
41. Zellweger,R. and Lopes,M. (2018) Dynamic architecture of eukaryotic DNA replication forks in vivo, visualized by electron microscopy. *Methods Mol. Biol.*, **1672**, 261–294.
42. Kumar,R., Gonzalez-Prieto,R., Xiao,Z., Verlaan-de Vries,M. and Vertegaal,A.C.O. (2017) The STUbL RNF4 regulates protein group SUMOylation by targeting the SUMO conjugation machinery. *Nat. Commun.*, **8**, 1809.
43. Sun,Y., Miller Jenkins,L.M., Su,Y.P., Nitiss,K.C., Nitiss,J.L. and Pommier,Y. (2020) A conserved SUMO pathway repairs topoisomerase DNA-protein cross-links by engaging ubiquitin-mediated proteasomal degradation. *Sci. Adv.*, **6**, eaba6290.
44. Dungrawala,H., Rose,K.L., Bhat,K.P., Mohni,K.N., Glick,G.G., Couch,F.B. and Cortez,D. (2015) The replication checkpoint prevents two types of fork collapse without regulating replisome stability. *Mol. Cell*, **59**, 998–1010.
45. Erker,Y., Neyret-Kahn,H., Seeler,J.S., Dejean,A., Atfi,A. and Levy,L. (2013) Arkadia, a novel SUMO-targeted ubiquitin ligase involved in PML degradation. *Mol. Cell. Biol.*, **33**, 2163–2177.
46. Poulsen,S.L., Hansen,R.K., Wagner,S.A., van Cuijk,L., van Belle,G.J., Streicher,W., Wikstrom,M., Choudhary,C., Houtsmuller,A.B., Marteijn,J.A. *et al.* (2013) RNF111/Arkadia is a SUMO-targeted ubiquitin ligase that facilitates the DNA damage response. *J. Cell Biol.*, **201**, 797–807.
47. van Cuijk,L., van Belle,G.J., Turkyilmaz,Y., Poulsen,S.L., Janssens,R.C., Theil,A.F., Sabatella,M., Lans,H., Mailand,N., Houtsmuller,A.B. *et al.* (2015) SUMO and ubiquitin-dependent XPC exchange drives nucleotide excision repair. *Nat. Commun.*, **6**, 7499.
48. Hendriks,I.A. and Vertegaal,A.C. (2016) A comprehensive compilation of SUMO proteomics. *Nat. Rev. Mol. Cell Biol.*, **17**, 581–595.
49. Schlacher,K., Christ,N., Siaud,N., Egashira,A., Wu,H. and Jasin,M. (2011) Double-strand break repair-independent role for BRCA2 in blocking stalled replication fork degradation by MRE11. *Cell*, **145**, 529–542.